A facility for PIV measurements of water hammer in pipe flow

Oldenziel, G.; Clemens, Francois

DOI
10.55037/lxlaser.21st.224

Publication date
2024

Document Version
Final published version

Published in
Proceedings of the 21st International Symposium on the Application of Laser and Imaging Techniques to Fluid Mechanics

Citation (APA)
Oldenziel, G., & Clemens, F. (2024). A facility for PIV measurements of water hammer in pipe flow. In *Proceedings of the 21st International Symposium on the Application of Laser and Imaging Techniques to Fluid Mechanics* Article 224 LISBON Simposia. https://doi.org/10.55037/lxlaser.21st.224

A FACILITY FOR PIV MEASUREMENTS OF MILD WATER HAMMER IN PIPE FLOW

G. Oldenziel[1,2,*], F. Clemens[3]

1: Deltares, The Netherlands
2: Laboratory for Aero & Hydrodynamics Delft University of Technology, The Netherlands
3: Dept. Civil and Environmental Engineering NTNU, Trondheim, Norway
*Corresponding author: gosse.oldenziel@deltares.nl

Keywords: PIV, pipe flow, water hammer, shock wave.

ABSTRACT

We present a facility for measurements of transient flow behavior due to rapid valve closure at initial Reynolds numbers up to $Re_\tau = 1237$. The facility allows the deployment of non-intrusive laser based diagnostic techniques such as Particle Image Velocimetry, Stereo Particle Image Velocimetry and Laser Doppler Anemometry. Steady state planar PIV and pressure drop measurements have been performed as well as planar PIV and absolute pressure measurements of the flow following rapid valve closure. The steady state measurements indicate that a clear logarithmic layer is present for the measured conditions at $Re_\tau > 344$ with a von-Kármán constant of k = 0.40. Resulting velocity and vorticity fields for an example transient case show the rich flow physics, including generation and advection of vorticity.

1. Introduction

For the design and analysis of pipeline systems, typically software is used in which the system is modelled 1-dimensional, where the mass and momentum equations are solved using the method of characteristics (MoC). In this approximation, the wall friction factor is mostly obtained from the well-known Moody chart for (steady) pipe flow. Often, water hammer related operational requirements of the system are of interest, such as minimum valve closure times to avoid excess pressures. Because the wall friction during the sudden deceleration and acceleration is not necessarily identical to the steady friction, see for example (Mathur et al., 2018), taking this into account may be of importance, depending on the design requirements. Often, the friction in case of such transient flows is approximated by the local instantaneous value for steady flow, this approach is referred to as the 'quasi-steady approximation'. The dissipation is known to be underestimated in this approach.

The flow in case of the passage of one or multiple water hammer shock waves is reminiscent of (a periodic version of) Stokes first problem (Schlichting, 1979), and thus the history of the flow has to be taken into consideration (Vardy & Brown, 2003). In daily engineering practice when using

large 1D numerical models, this can lead to impracticalities such as long calculation times, so also models in which this dependence on the history is simplified could be of interest (Abdeldayem et al., 2021). Even in the history-dependant models, such as the model described by (Vardy & Brown, 2003), already assumptions are made that are simplifying the flow physics considerably, such as the assumption of a constant eddie viscosity ν_t. Therefore, one of the goals of the current facility, is to assess existing models for friction, and specifically the assumptions in these models, during fast transient water hammer events against experimental data, and improve current models and understanding.

The pressure difference Δp over a water hammer shock wave depends on the water hammer shock wave speed c, the density of the fluid ρ, and the bulk velocity difference ΔU_b and can be estimated as:

$$\Delta p = c\rho\Delta U_b \tag{1}$$

and is known as the Joukowski pressure. The water hammer shock wave speed depends additionally on the liquid bulk modulus K, pipe properties such as the Young's modulus E, the wall thickness e and the diameter D as:

$$c = \sqrt{\frac{K/\rho}{1 + [(K/E)(D/e)]c_1}} \tag{2}$$

where the factor c_1 depends on the anchoring and the Poisson coefficient ν, see (Klein et al., 2023). Note that these expressions are simplified versions of the expressions of the theory of fluid structure interaction (FSI), see (Skalak, 1956; Tijsseling et al., 2008). The extended theory also leads to expressions for the so-called precursor wave speed, see for example (Ando et al., 2011; Cornel et al., 2023; Capanna & Bardet, 2021).

In this paper, we present a facility that allows the deployment of non-intrusive laser based techniques, such as Particle Image Velocimetry (PIV), Stereo Particle Image Velocimetry (SPIV) (Adrian & Westerweel, 2011) and Laser Doppler Anemometry (LDA) for measurements of water hammer in pipe flow.

2. Experimental Set-Up and conditions

A facility was designed and built at Deltares (Delft, The Netherlands); see Figure 1. The facility is a water-filled pipe with a length of 27 m. The water level at the up- and downstream ends of the pipe is maintained via overflow boundaries connected to a separate reservoir. The up- and downstream tanks are placed at elevations and the internal overflow boundaries are at 1.93 m and 1.25 m above the pipe centerline. From the upstream reservoir a PVC pipe section with a diameter of 100 mm leads the working fluid to the PMMA measurement section via a contraction with a ratio of 1:14.7. The measurement section has a diameter of 88.2 mm and a length of 16.8 m, a wall thickness of 6.0 mm and is anchored using circular clamps onto a steel beam which is clamped

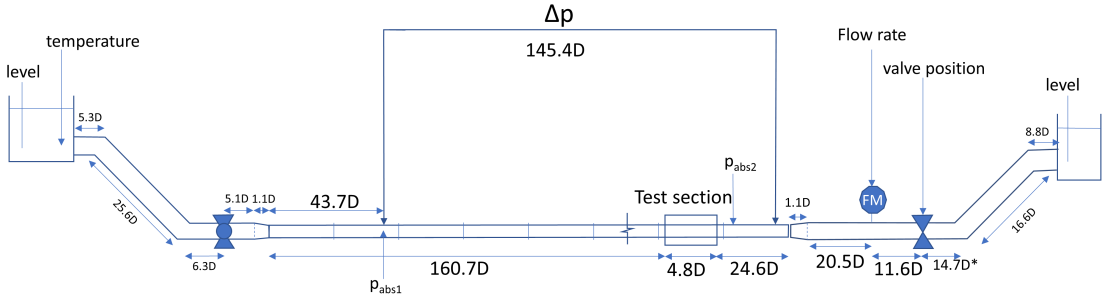

Figure 1. Sketch of pipe flow facility with indications of sensor locations and PIV test section. Note that all lengths are related to the diameter D of the measurement section (88.2 mm). The water level at the up- and downstream ends of the pipe is maintained via overflow boundaries connected to a separate reservoir which is not shown in the Figure. The symbol Δp indicates the connections of the differential pressure sensor.

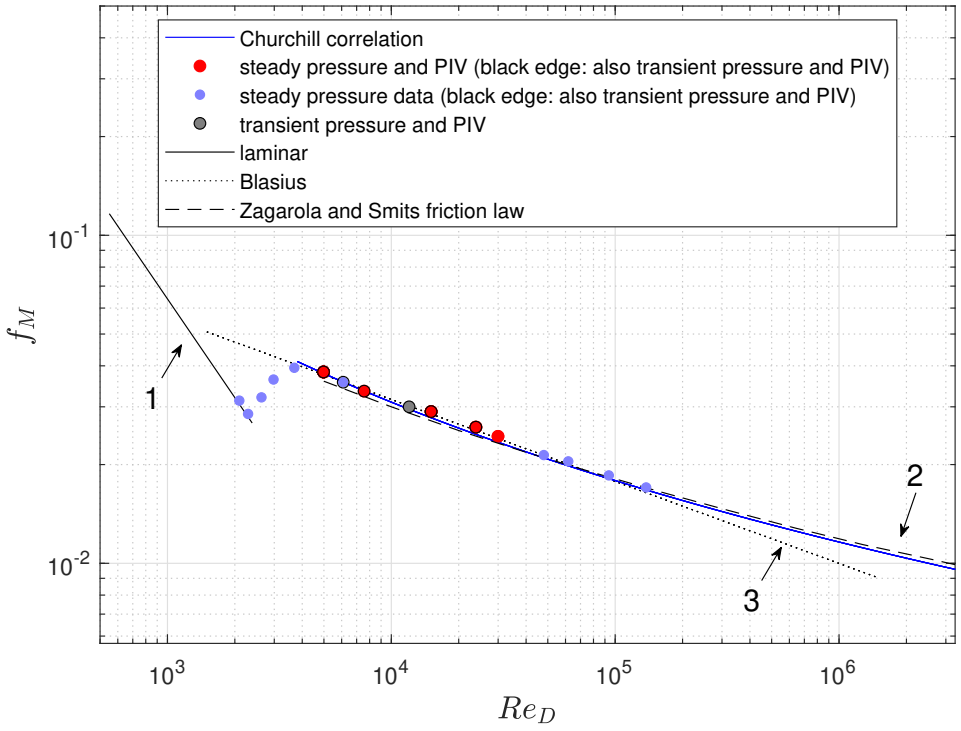

Figure 2. Friction factor as measured in the pipe flow facility as a function of the Reynolds number $Re_D = U_b D/\nu$. The lines represent: 1 the friction factor for laminar Poiseuille flow ($f_M = 64/\mathrm{Re}_D$); 2 the friction law for a smooth wall, (Zagarola & Smits, 1998); 3 the Blasius friction law ($f_M = 0.316\mathrm{Re}_D^{-1/4}$). Red dots indicate measurements where simultaneous pressure drop and steady state PIV measurements are performed, symbols with a black edge indicate that a transient PIV measurement is performed. The grey marker indicates a measurement where the pressure difference is based on the initial part of the transient measurement. The steady pressure data indicates that for the present flow rates the pipe is hydraulically smooth.

to steel boxes of approximately 0.7 $\times$ 1.0 $\times$ 1.0 m filled with heavy square rock elements. The modulus of elasticity of the PMMA measurement section was measured in a compression test to be 2993 MPa and the Poisson ratio was measured to be $\nu_{Poisson} = 0.42$. The measurement section is equipped with a transparent rectangular box suitable for 2D PIV, SPIV and LDA near the downstream end, see section 2.3. The measurement section is essentially based upon the pipe described in Draad & Nieuwstadt (1998); Draad (1998); Draad et al. (1998), with dedicated flanges to ensure smoothly connected pipe sections. Two pressure transducers (Druck Unik 5000 PDCR-5031, frequency response up to 3.5 kHz) are used for the pressure measurements. The upstream sensor is located 43.7 D downstream of the contraction, and the second pressure transducer is located 5.7 D downstream of the field of view of the PIV camera. Both sensors are mounted at the side of the pipe. A differential pressure sensor (Rosemount 3051, with a range of 7.5 mBar for measurements up to $Re_D = U_b D/\nu = 30000$, and a second Rosemount 3051 sensor with a larger range of 60 mBar, for measurements at $Re_D > 30000$) is used to quantify the pressure difference over 145.4 D. The upstream connection of this sensor is located opposite of the connection of the upstream pressure sensor. The downstream connection 23.2 D downstream of the PIV section. Note that the location of the upstream connection of the differential pressure sensor only allows for fully developed laminar flow up to $Re_D = 733$ but fully developed turbulent flow exists up to $Re_D = 1 \times 10^6$, see Chaudhury et al. (2015). 24.6 D downstream of the PIV section an expansion section (identical to the contraction, ratio 1:14.7) leads to the downstream PVC section with an internal diameter of $D = 100$ mm, with a flow meter (Endress and Hauser ProMag 33F). Downstream of the flow meter a butterfly valve with an internal diameter of 100 mm is located (Wouter Witzel rubber lined EVML). This valve is used to regulate the flow and generate sudden flow deceleration events, see section 2.2. Downstream of the valve the flow is connected with the downstream tank via a $D = 100$ mm PVC pipe section. Note that in the facility no honeycomb structure for flow straightening is present because this will interfere with the shock wave behavior and also no contraction is present inside the upstream tank.

2.1. Pressure drop measurements

Pressure drop measurements have been performed to quantify the flow. The differential pressure data is sampled at 20 Hz over 1000 s and compensated for the measured static pressure difference at 15 flow rates between $Re_D = 2094$ and $Re_D = 137522$.

In Figure 2 we show the friction coefficient based on the measured pressure gradient and measured bulk flow rate. Based on the pressure data, transition from laminar to turbulent flow appears to occur between $Re_D = 2292$ and $Re_D = 4979$. The data indicates that for the present range in Re_D, the pipe is hydraulically smooth.

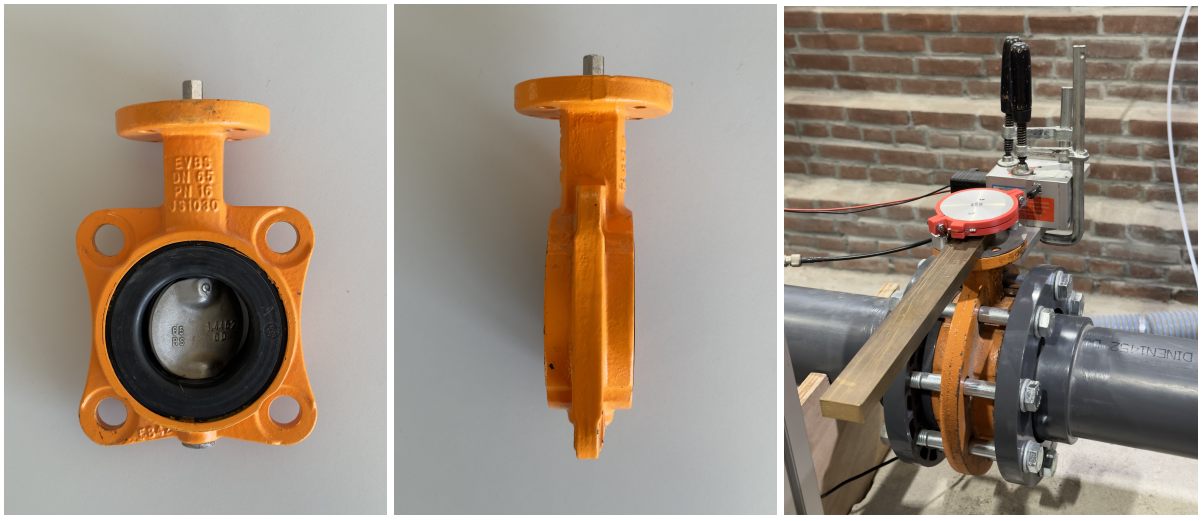

Figure 3. Left and center panel: Wouter Witzel rubber lined EVBS valve. Note that the depicted valve is slightly different from the installed valve and has a diameter of 65 mm instead of 100 mm. Right panel: valve as installed in the facility with actuator arm and wire-potentiometer for position measurement.

2.2. Valve, valve actuation and sensor data acquisition

The valve used to impulsively decelerate the flow is shown in 3. The valve in the facility is in the downstream pipe section of $D = 100$ mm and is of butterfly type (Wouter Witzel rubber lined EVBS). For a quantification of a ball valve, see Ferreira et al. (2018). In order to generate the sequence of rapidly decelerating and accelerating flow that is characteristic of the sudden imposition of a zero-mass flow boundary condition downstream and a constant pressure condition upstream and to quantify the valve closure time, the valve position downstream of the measurement section is quantified using a wire potentiometer. The valve is operated using a magnetically actuated, gravity driven aluminium arm with a length of approximately 1.5 m from below its hinge. The hinge is located directly above the valve. The arm impacts on the valve actuator arm, to close the valve promptly.

All data except the PIV data is acquired using dedicated LabView software. For the steady state data, the acquisition rate is 20 Hz. For the transient measurements all sensor data, except the PIV data, is acquired at a sample rate of 10 kHz.

2.3. PIV setup and processing

The PIV section consists of a rectangular water-filled box that encloses the pipe. An arrangement of external and internal slits avoids serious light refraction from the curved pipe wall for the case that the light sheet is oriented in the vertical-axial-plane as is the case for the present measurements. Two liquid filled prisms are present on one side of the box to accommodate stereo-PIV measurements in a vertical plane oriented perpendicular to the pipe axis. The flow was seeded with 10 μm diameter tracer particles (Sphericel 110P8, Potters Industries Inc.) and illuminated with a light

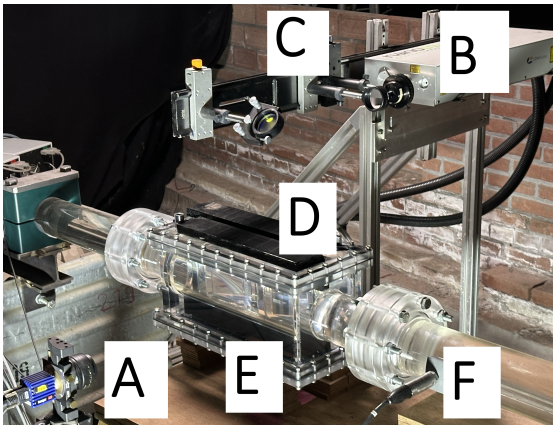

Figure 4. PIV section, with camera (A), laser (B), light sheet optics (C), external (D) and internal slits (E) (note that the beam stop is removed the picture). A pressure transducer (F) is visible immediately downstream of the PIV section.

sheet with a thickness estimated to be < 1.0 mm, generated from the beam of a frequency-doubled dual Nd:YAG laser (Litron Nano L PIV 50-100). Images were recorded using a CMOS camera (LaVision ImagerMX 4M, 2048×2048 pixels with 5.5 μm pixel pitch) equipped with a 50 mm lens (Micro Nikkor) using a f/5.6 aperture stop. For the steady flow measurements the framing rate was 1 Hz whereas for the transient measurements the framing rate is 60 Hz. The exposure time delay was between 6500 μs and 1300 μs for the steady flow cases and between 6500 μs and 1500 μs for the transient cases. The image magnification was $M_0 = 0.12$. The recorded images were pre-processed using a 5×5-px minmax filter (Adrian & Westerweel, 2011) to enhance the image contrast and to reduce the number of spurious vectors. Despite the internal and external slits, remnants of the internal reflections, which occur as thin horizontal lines near locations $|r| = 0.26D$, however, are occasionally visible in the data.

The PIV processing for the steady flow cases is performed at a window size of 32×32 pixel interrogation windows with 50% overlap. For vector validation a peak ratio of 1.5 is required between the highest and second highest correlation peak and universal outlier detection is applied where a maximum residual of 2 is allowed, see Westerweel & Scarano (2005). Invalid vectors are replaced by a linearly interpolated vector. The percentage of valid vectors is typically larger than 97%. A fourth order polynomial calibration method is used, see Adrian & Westerweel (2011). The processing is performed using the PIV ware Matlab software Adrian & Westerweel (2011). For the preliminary results for the transient cases the PIV processing is performed at a window size of 16×16 pixel interrogation windows with 50% overlap using LaVision Davis software version 8 .

The synchronisation of the PIV data with the other sensor data was performed by extending the camera trigger TTL pulse of 5 μs to 10000 μs using a signal processing unit (HP 33120A) and recording this in the data acquisition.

Table 1. The flow conditions and exposure time delay for the measurements. The data for case D4 is based on the initial part of the transient measurement.

Case	U_b (m/s)	Re_τ	Re_D	Δ t$_{PIV}$ (μs)	t$_{close}$ (ms)	ν/u_τ (mm)
S1	0.052	344	5037	6500	-	0.256
D1				6500	36	
D2	0.063	405	6110	6500	38	0.218
S3	0.084	512	7999	4500	-	0.172
D3				4000	32	
D4	0.123	705	11533	2500	37	0.125
S5	0.166	904	15391	2700	-	0.098
D5				2200	40	
S6	0.247	1237	22009	1600	-	0.071
D6				1500	50	
S7	0.329	1621	29916	1300	-	0.054

2.4. Experimental conditions

The experimental for all steady and transient cases are indicated in Table 1. The steady flow is measured at five flow rates using PIV and differential pressure measurements between $Re_\tau = 344$ and $Re_\tau = 1621$, and transient valve closure flow behavior is measured using PIV and regular pressure sensors between $Re_\tau = 344$ and $Re_\tau = 1237$.

3. Results

3.1. Steady flow

For steady flow 1000 PIV images were recorded for each case. Figure 5 shows the measured axial velocity profiles for the steady cases between $Re_\tau = 344$ and $Re_\tau = 1621$ in linear and logarithmic scaling. Upon comparing with the measured flow rate the maximum difference in bulk velocity is 2.2% for case S1 and less for the other cases.

The right panel of Figure 5 shows the velocity profiles for all Reynolds numbers, but now in a semi-log plot. It is observed that the range in the log-region increases with Re_τ and that the profile agrees with a logarithmic profile with a von-Kármán constant of k = 0.40. For $Re_\tau = 344$ there is almost no log region present.

It can be observed that the facility enables measurements of near wall velocity profiles at a data spacing of $\Delta r = 0.762$ mm. In the next section, an example of a case involving a water hammer shock wave is given.

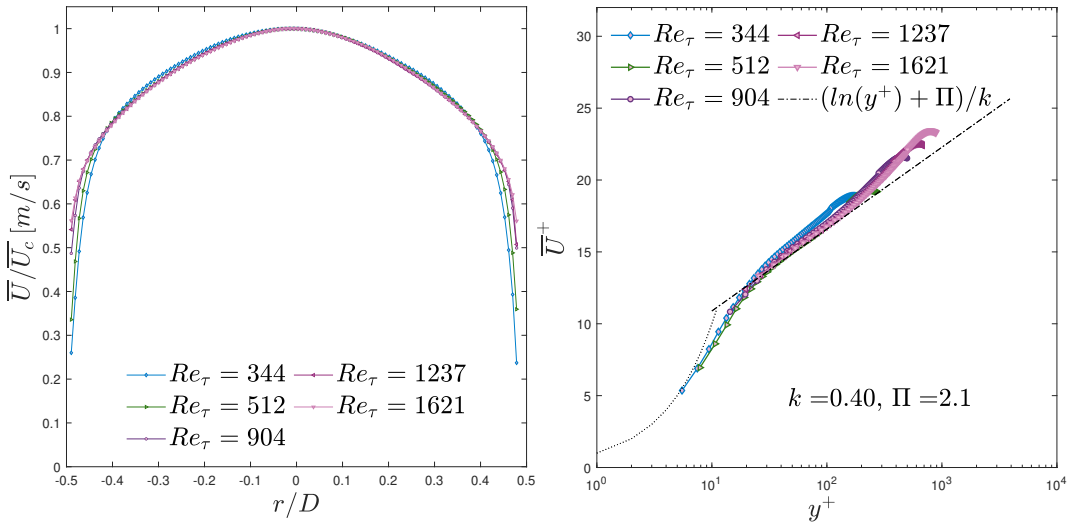

Figure 5. Left: measured mean axial velocity profiles for steady flow between $Re_\tau = 344$ and $Re_\tau = 1621$. Right: The mean axial velocity profile in wall units for all values of Re_τ. The dash-dotted line indicates $(\ln y^+ + \Pi)/k$ where $\Pi = 2.1$ and $k = 0.40$. Note that the measurements of the rapid valve closure events are performed up to an initial $Re_{\tau,in} = 1237$ to prevent structural damage to the facility.

3.2. Transient flow

For six cases, with initial Reynolds numbers from $Re_{\tau,in} = 344$ to $Re_{\tau,in} = 1237$, 1000 PIV images and accompanying sensor data are recorded for valve closure events. .

3.2.1. valve, pressure and wave speed

Figure 6 shows the valve position, the pressure and the measured shock wave speed c. The valve closure time is determined as the time between the moment when the position attains values below 90% of the initial setting until when the position becomes smaller than 10% of the final value (0% open). This leads to valve closure times between $\Delta t_{close} = 36$ ms and $\Delta t_{close} = 50$ ms.

The pressure is shown for the cases D1 to D6 in Figure 6. A decaying oscillatory pressure behavior is observed as is typical for events where suddenly the downstream mass flow is imposed, in combination with a constant upstream pressure (Klein et al., 2023). Because the change in water hammer shock wave speed between the downstream PVC and PMMA pipe sections, part of the initial shock wave is reflected at the transition location and part is transmitted, leading to a stepwise increase of the pressure until the maximum pressure occurs. The maximum measured absolute pressure is 1.35 Bar and the minimum pressure is -0.74 Bar for case D6. Additionally, the presence of two values of the shock wave speed is observable in the existence of multiple maxima after some time.

The water hammer shock wave speed c is determined by estimating the travel time between the leading flanks of the pressure signals for threshold values of 20%, 30% and 40% of the maximum

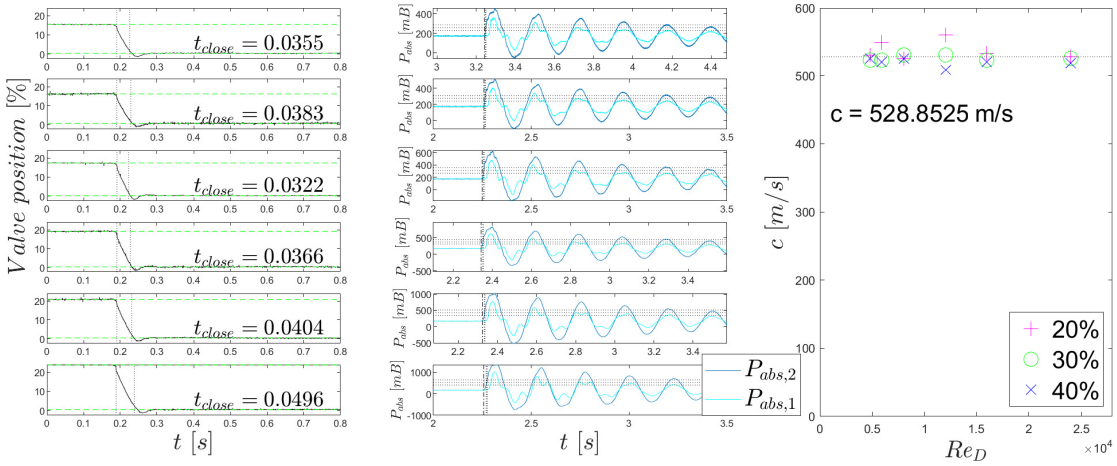

Figure 6. Left panel: valve position. From top to bottom: case D1 to D6. Center panel: pressure. From top to bottom: case D1 to D6. Right panel: shock wave speed. The black dash-dotted vertical line indicates the instant when the absolute pressure exceeds 200 mBar. The dotted horizontal lines indicate the instant when the pressure increase exceeds 20%, 30% and 40% of the maximum pressure increase.

value and dividing by the distance between the sensors. The results are shown in Figure 6, where no dependence on the Reynolds number is found and c is determined by the average of all values, leading to $c = 529$ m/s.

3.2.2. Instantaneous U_b and vorticity

In Figure 7 we present an example result for the instantaneous bulk velocity for case D6, measured using PIV. The velocity behavior oscillates with a decaying amplitude and it is observed that the liquid initially undergoes a rapid deceleration until approximately $U_b = 0$ m/s before decelerating further to -0.16 m/s and accelerating to 0.19 m/s and decaying further.

Instantaneous vorticity fields, velocity profiles and vorticity profiles for case D6 are shown in Figure 8 and in in Figure 9.

The sudden deceleration causes the axial velocity to decrease by almost 0.45 m/s over almost the full diameter of the pipe except near the wall where the no-slip condition is met, as is visible in panels 1 and 2 in Figure 8.

During periods one and two of oscillation the shear caused by the large velocity gradients near the wall forms vortices and a large scale circulating flow that is oriented in the downstream direction near the pipe center and in the upstream direction near the pipe wall starts to form.

Near the third period of oscillation the pre-existing vorticity, possibly heads of hairpin vortices (Adrian et al. (2000)), and the additional vorticity that is generated near the wall have been advected by the large scale circulating flow and merge into three vortices near location $r = 0.30$ mm, as shown in panels 6 to 8 in Figure 8. Near the bottom wall also generation and advection of

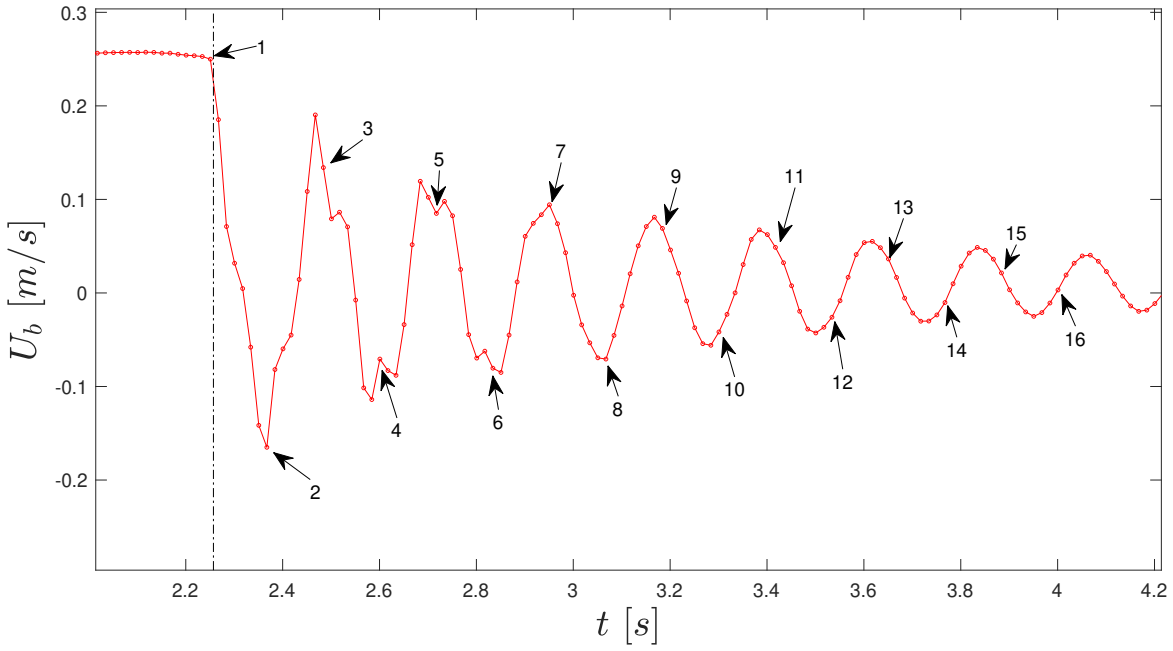

Figure 7. Measured bulk flow rate versus time for transient case D6. The black dash-dotted vertical line indicates the instant when the absolute pressure exceeds 200 mBar. The numbers refer to the images in Figure 8 and 9

.

vorticity occurs.

From the fourth period of oscillation onwards, the three vortices near $r = 0.30$ mm break up and the most intense vorticity is dissipated as shown in panels 13 to 16 in Figure 9.

4. Conclusions

We present a facility for measurements of transient flow behavior due to rapid valve closure at initial Reynolds numbers up to $Re_\tau = 1237$. The facility allows the deployment of non-intrusive laser based diagnostic techniques such as Particle Image Velocimetry, Stereo Particle Image Velocimetry and Laser Doppler Anemometry. Steady state planar PIV and pressure drop measurements have been performed as well as planar PIV and absolute pressure measurements of the flow following rapid valve closure. The steady state measurements indicate that a clear logarithmic layer is present for the measured conditions at $Re_\tau > 344$ with a von-Kármán constant of k = 0.40. Resulting velocity and vorticity fields for an example transient case show the rich flow physics, including generation and advection of vorticity.

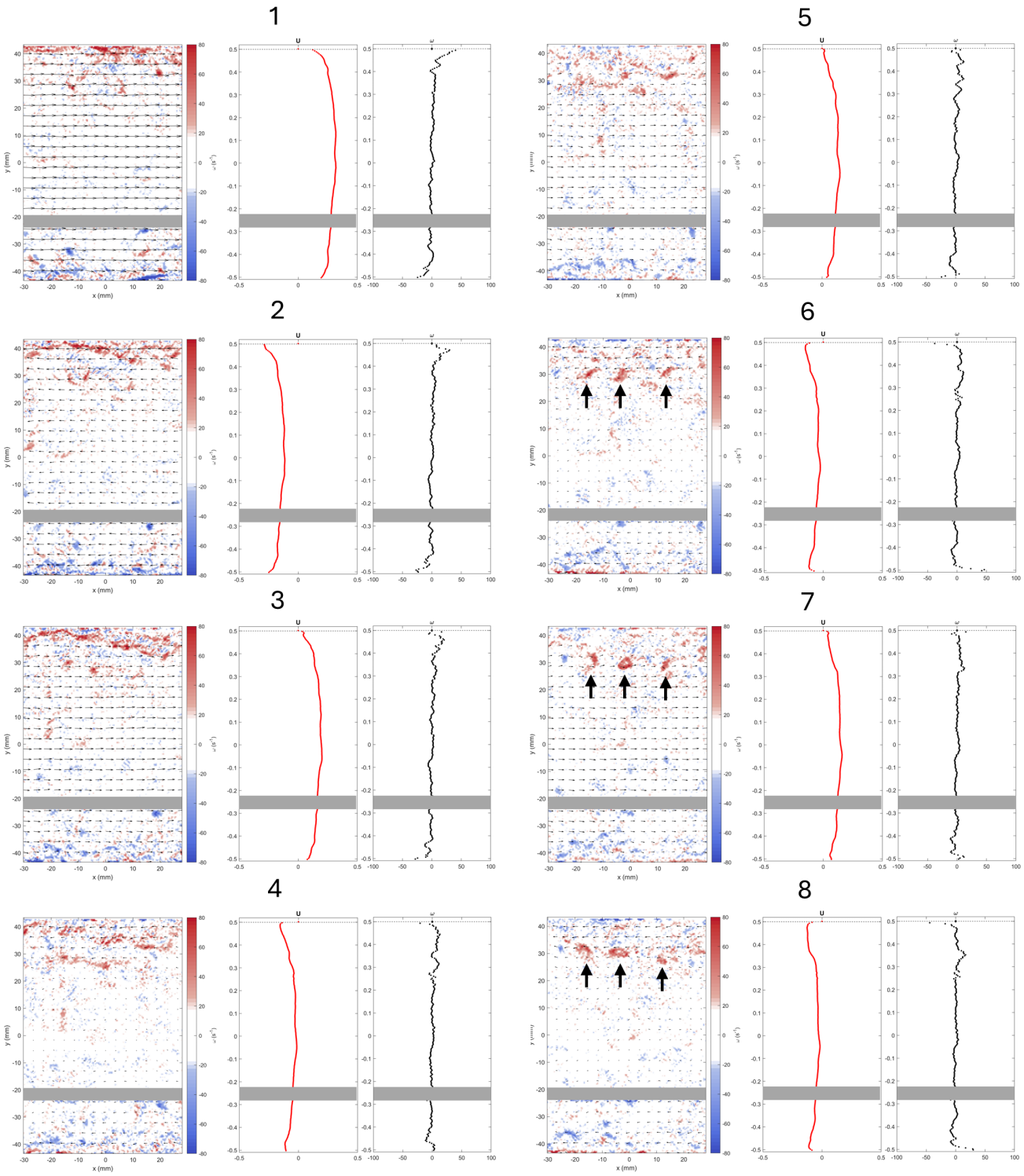

Figure 8. Sequence of every seventh vorticity field for the measurement in Figure 7 part 1: first three periods. The red lines indicate the axial velocity. The black lines indicate the vorticity. The black arrows indicate vortices that are referred to in the text. The numbers refer to the arrows in Figure 7. One in every 10 vectors is shown. The grey area is masked.

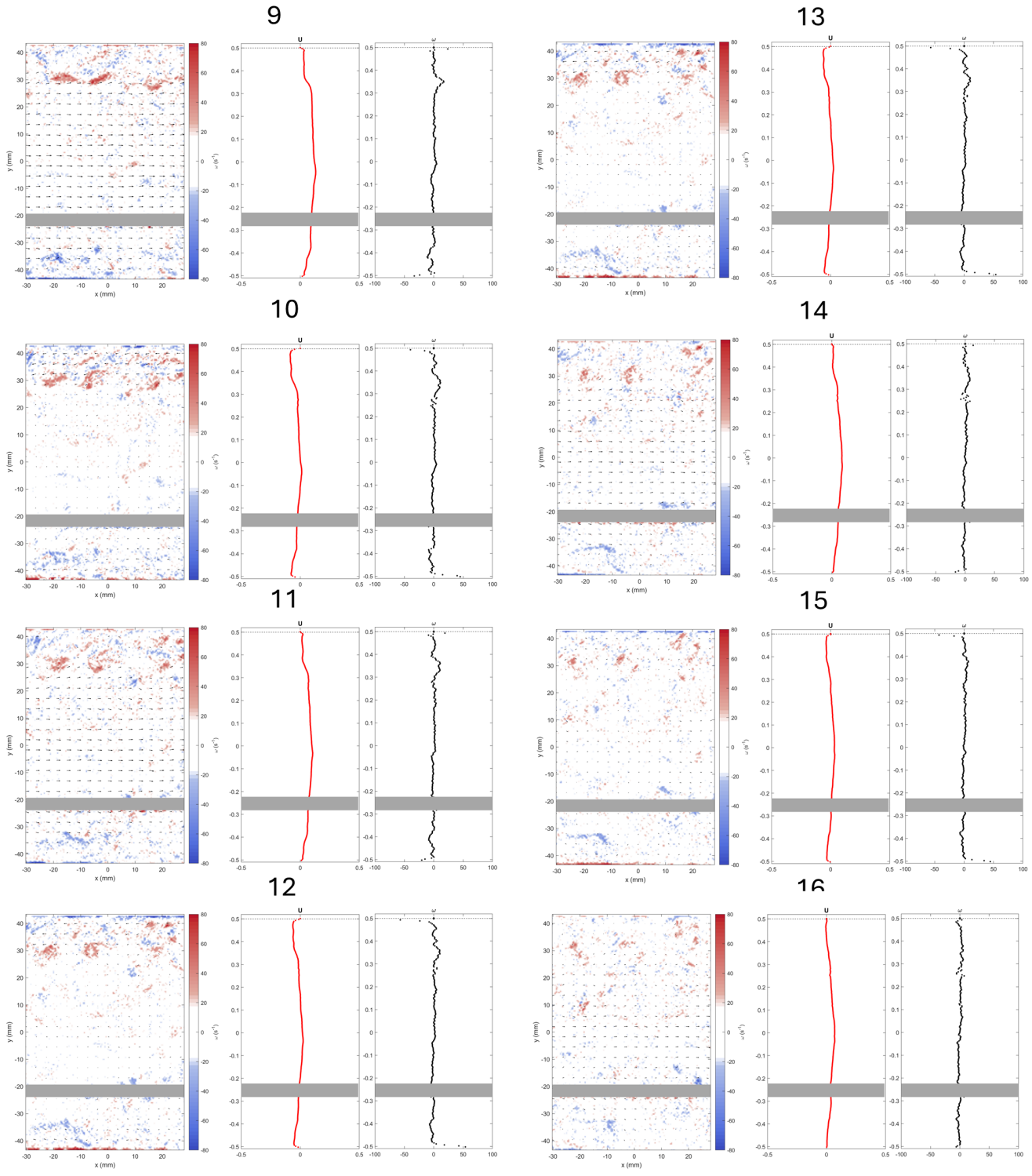

Figure 9. Sequence of every seventh vorticity field for the measurement in Figure 7 part 2: period four to eight. The red lines indicate the axial velocity. The black lines indicate the vorticity. The numbers refer to the arrows in Figure 7. One in every 10 vectors is shown. The grey area is masked.

4.1. Acknowledgements

This research was funded by the Top Sector Alliance for Knowledge and Innovation (TKI) Water Technology (Dutch Ministry of Economic Affairs and Climate policy, grant 2021DEL004), and supported by Ingenieursbureau Rotterdam.

The authors would like to thank the whole department of Experimental Facility Support for the support and good working atmosphere. The authors would also like to thank prof. Akke Suiker from TU Eindhoven for the characterisation of the material parameters of the pipe, Alex Duinmeijer, prof. Jerry Westerweel, Edwin Overmars and the Laboratory for Aero- and Hydrodynamics at TU Delft and the full (previous and current) members of the Measurements and Monitoring and Hydraulics of Pipeline Systems teams at Deltares, Bas van Vossen and Jelle Jagtenberg.

References

Abdeldayem, O. M., Ferràs, D., van der Zwan, S., & Kennedy, M. (2021). Analysis of unsteady friction models used in engineering software for water hammer analysis: Implementation case in wanda. *Water*, *13*(4), 495.

Adrian, R. J., Meinhart, C. D., & Tomkins, C. D. (2000). Vortex organization in the outer region of the turbulent boundary layer. *J. Fluid Mech.*, *422*, 1-54.

Adrian, R. J., & Westerweel, J. (2011). *Particle Image Velocimetry*. Cambridge University Press.

Ando, K., Sanada, T., Inaba, K., Damazo, J., Shepherd, J., Colonius, T., & Brennen, C. (2011). Shock propagation through a bubbly liquid in a deformable tube. *Journal of Fluid Mechanics*, *671*, 339–363.

Capanna, R., & Bardet, P. M. (2021). High speed piv measurements in water hammer. In *14th international symposium on particle image velocimetry* (Vol. 1).

Chaudhury, R. A., Herrmann, M., Frakes, D. H., & Adrian, R. J. (2015). Length and time for development of laminar flow in tubes following a step increase of volume flux. *Exp. Fluids*, *56*, 22.

Cornel, W. A., Westerweel, J., & Poelma, C. (2023). Non-intrusive, imaging-based method for shock wave characterization in bubbly gas–liquid fluids. *Experiments in Fluids*, *64*(2), 35.

Draad, A. A. (1998). *Laminar-turbulent transition in pipe flow for Newtonian and non-Newtonian fluids* (Unpublished doctoral dissertation). Delft University of Technology.

Draad, A. A., Kuiken, G. D. C., & Nieuwstadt, F. T. M. (1998). Laminar-turbulent transition in pipe flow for Newtonian and non-Newtonian fluids. *J. Fluid Mech.*, *377*, 267-312.

Draad, A. A., & Nieuwstadt, F. T. M. (1998). The earth's rotation and laminar pipe flow. *J. Fluid Mech.*, *361*, 297-308.

Ferreira, J. P. B., Martins, N. M., & Covas, D. I. (2018). Ball valve behavior under steady and unsteady conditions. *Journal of Hydraulic Engineering*, *144*(4), 04018005.

Klein, S., Traudt, T., & Oschwald, M. (2023). Comparison of water and cryogenic fluid hammer experiments for rocket engine feed line systems. *Experiments in Fluids*, *64*(2), 30.

Mathur, A., Gorji, S., He, S., Seddighi, M., Vardy, A., O'Donoghue, T., & Pokrajac, D. (2018). Temporal acceleration of a turbulent channel flow. *Journal of Fluid Mechanics*, *835*, 471–490.

Schlichting, H. (1979). *Boundary-layer theory* (7th ed.). New York, NY: McGraw-Hill.

Skalak, R. (1956). An extension of the theory of water hammer. *Transactions of the American Society of Mechanical Engineers*, *78*(1), 105–115.

Tijsseling, A. S., Lambert, M. F., Simpson, A. R., Stephens, M. L., Vítkovskỳ, J. P., & Bergant, A. (2008). Skalak's extended theory of water hammer. *Journal of sound and vibration*, *310*(3), 718–728.

Vardy, A., & Brown, J. (2003). Transient turbulent friction in smooth pipe flows. *Journal of sound and vibration*, *259*(5), 1011–1036.

Westerweel, J., & Scarano, F. (2005). Universal outlier detection for PIV data. *Exp. Fluids*, *39*, 1096-1100.

Zagarola, M. V., & Smits, A. J. (1998). Mean-flow scaling of turbulent pipe flow. *J. Fluid Mech.*, *373*, 33-79.